Supporting Information

Deciphering cycling voltage dependent failures of O3-layered cathode for sodium ion battery

Xuejiao Zhao[1], Lihan Zhang[1], Xiaoqi Wang*[,2], Jinhui Li[1], Lin Zhang[2], Di Liu[2], Rui Yang[2], Xu Jin[2], Manling Sui[1], Pengfei Yan*[,1]

[1] Beijing Key Laboratory of Microstructure and Property of Solids, Faculty of Materials and Manufacturing, Beijing University of Technology, Beijing 100124, China.

[2] PetroChina Research Institute of Petroleum Exploration & Development, Beijing 100083, China.

*** Corresponding Authors**

Xiaoqi Wang: wangxq07@petrochina.com.cn; Pengfei Yan: pfyan@bjut.edu.cn

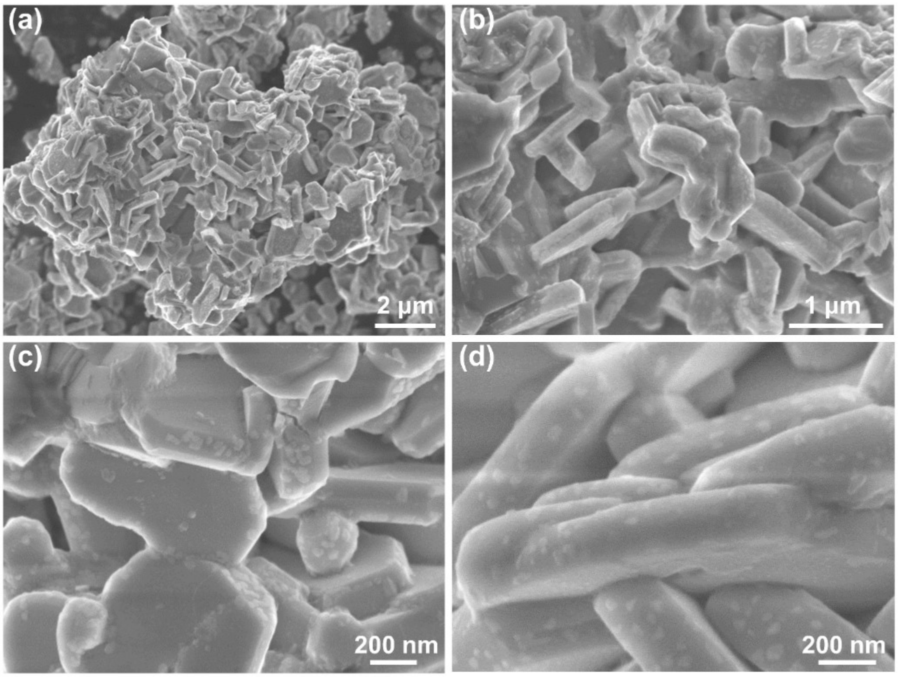

Figure S1. SEM images of the NFM sample. **(a, b)** low and **(c, d)** high magnification SEM images of the NFM.

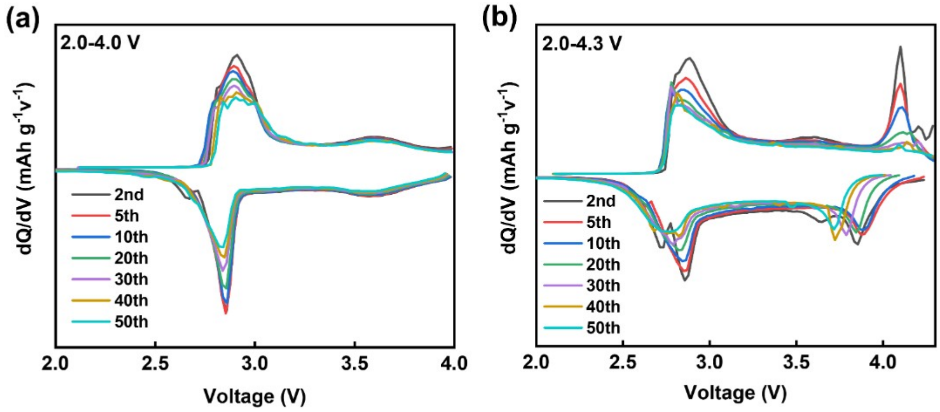

Figure S2. dQ/dV profiles of the NFM cathode upon **(a)** 2.0-4.0 V and **(b)** 2.0-4.3 V cycling.

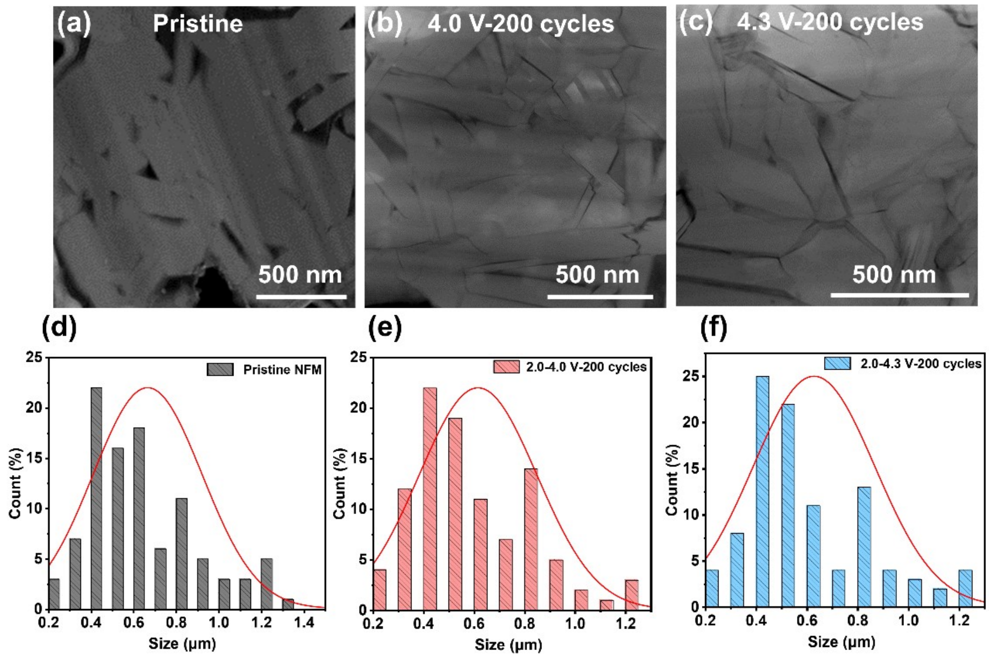

Figure S3. **(a-c)** STEM-HAADF images of NFM sample before and after cycling. **(d-e)** Normalized grain size distribution of the primary particles before and after cycling. **(a, d)** Pristine NFM, **(b, e)** after 200 cycles in the voltage ranges of 2.0-4.0 V, **(c, f)** after 200 cycles in the voltage ranges of 2.0-4.3 V.

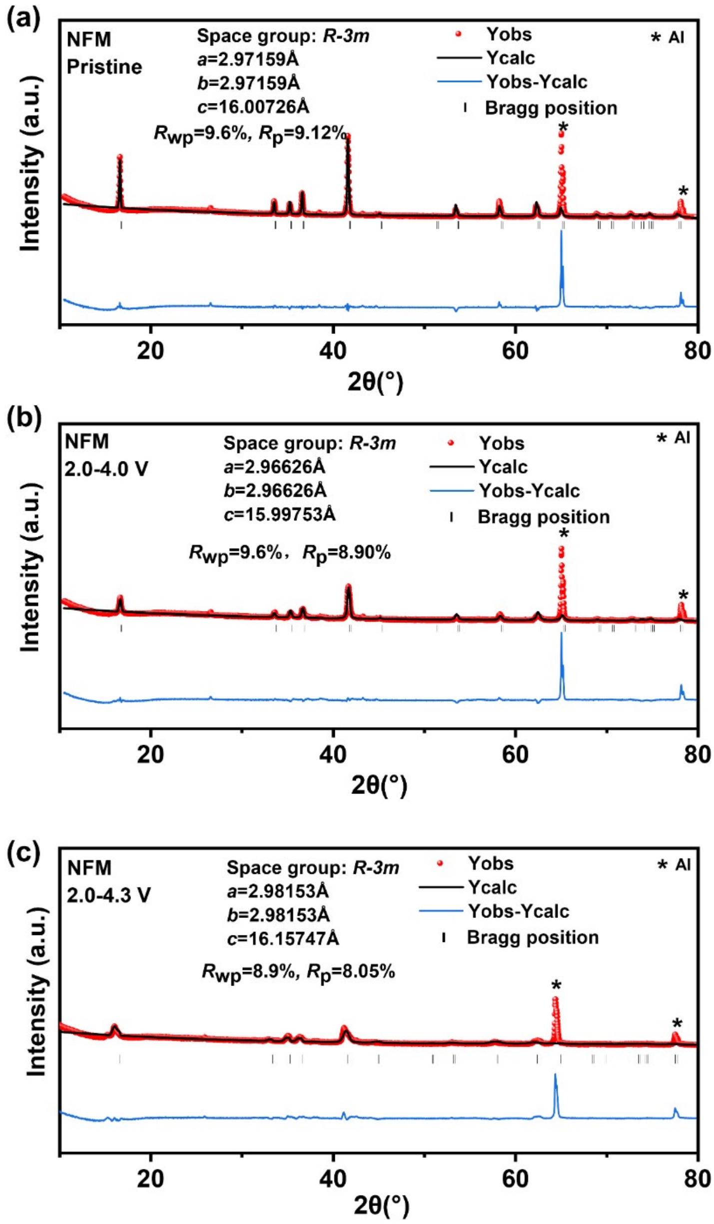

Figure S4. XRD Rietveld refinement results of the NFM cathode. **(a)** pristine, **(b)** after 200 cycles in the voltage range of 2.0-4.0 V, **(c)** after 200 cycles in the voltage range of 2.0-4.3 V.

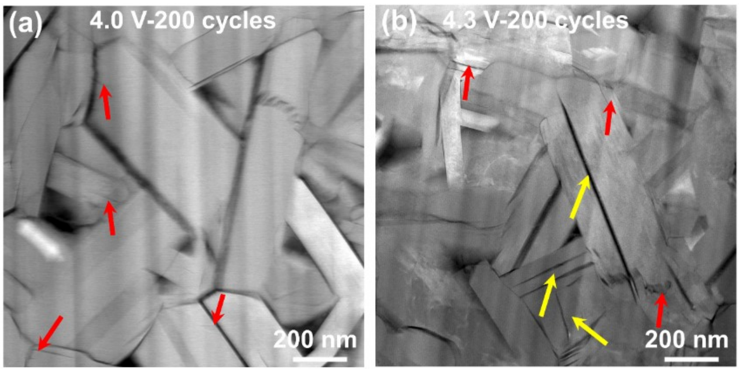

Figure S5. STEM-HAADF images of the NFM cathode after 200 cycles at different cutoff voltages. **(a)** 4.0 V, **(b)** 4.3 V. The red arrows indicate surface cracks, and the yellow arrows represent intragranular cracks.

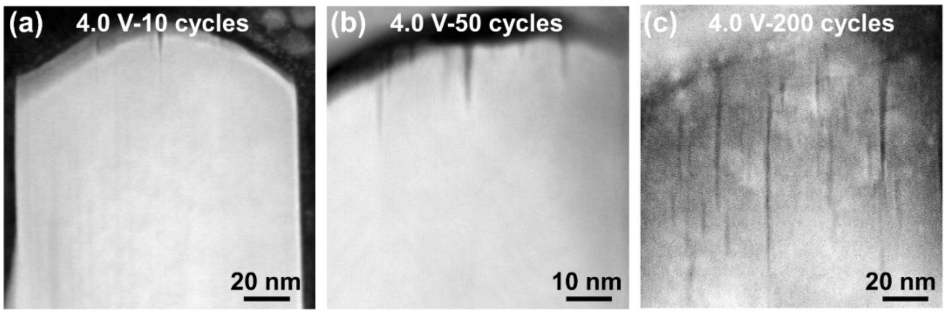

Figure S6. STEM-HAADF images showing surface crack evolution with increasing cycling numbers at 2.0-4.0 V. **(a)** 10 cycles, **(b)** 50 cycles, **(c)** 200 cycles.

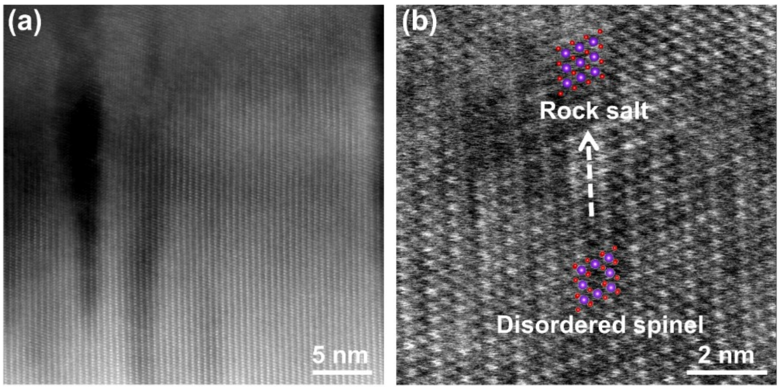

Figure S7. **(a)** High-magnification STEM-HAADF image of surface crack after 200 cycles in the voltage range of 2.0-4.0 V. **(b)** Lattice structure in the surface crack region.

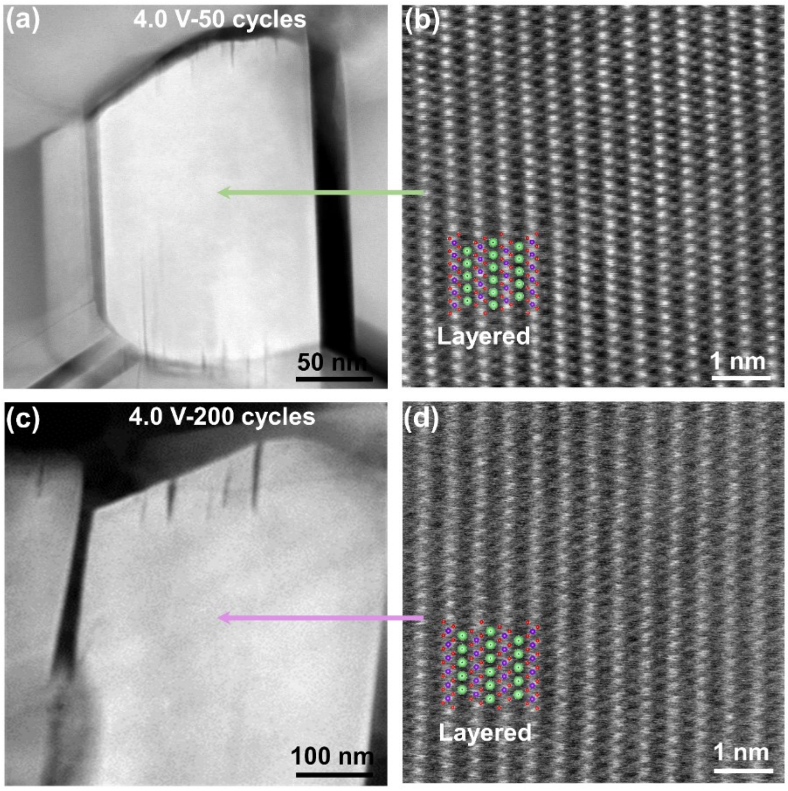

Figure S8. STEM-HAADF images of the NFM sample after cycling. **(a)** 50 cycles, **(c)** 200 cycles. **(b, d)** High resolution lattice images from the grain bulk showing the inner bulk lattice remains layered structure after cycling.

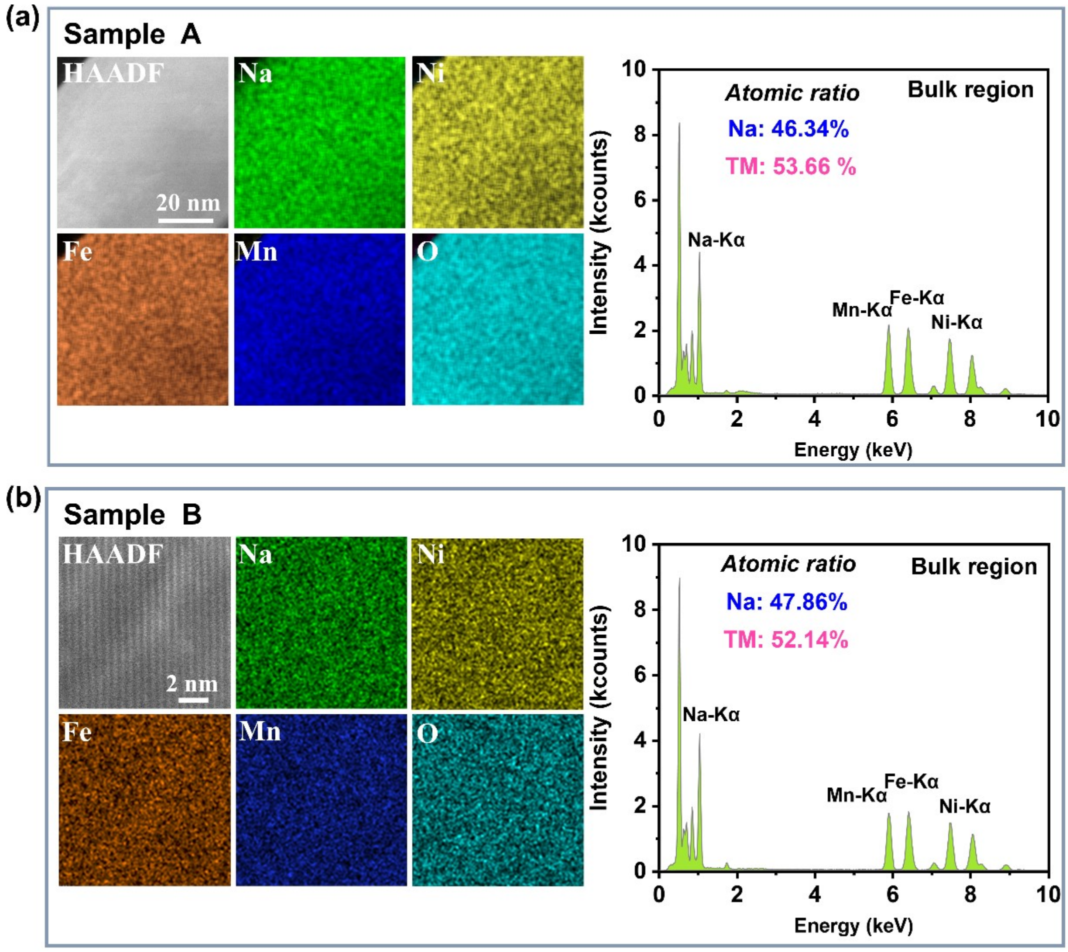

Figure S9. STEM-HAADF images, EDS elemental mappings of Na, Ni, Fe, Mn, and corresponding spectra of sample A **(a)** and sample B **(b)**, showing grain interior with uniform elemental distribution after 200 cycles in the voltage range of 2.0-4.0 V.

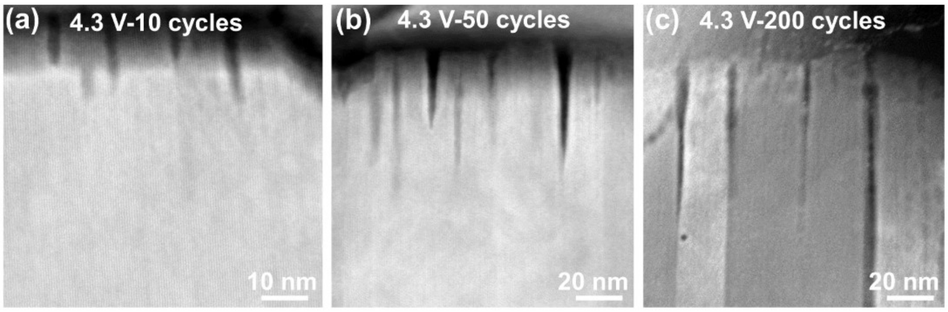

Figure S10. STEM-HAADF images showing surface crack evolution with increasing cycling numbers at 2.0-4.3 V. **(a)** 10 cycles, **(b)** 50 cycles, **(c)** 200 cycles.

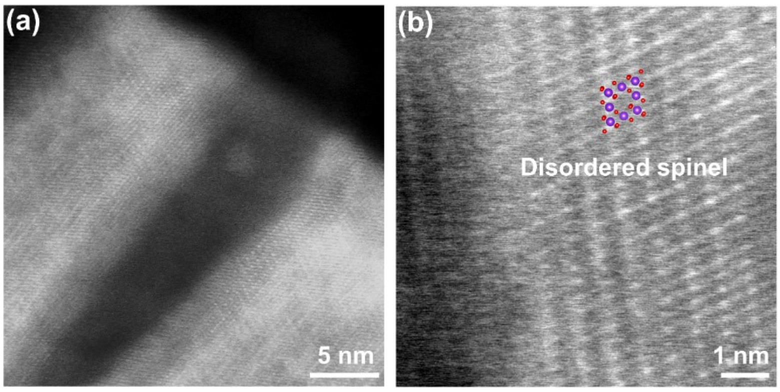

Figure S11. **(a)** High-magnification STEM-HAADF image of surface crack after 200 cycles in the voltage range of 2.0-4.3 V. **(b)** Lattice structure from the crack surface region.

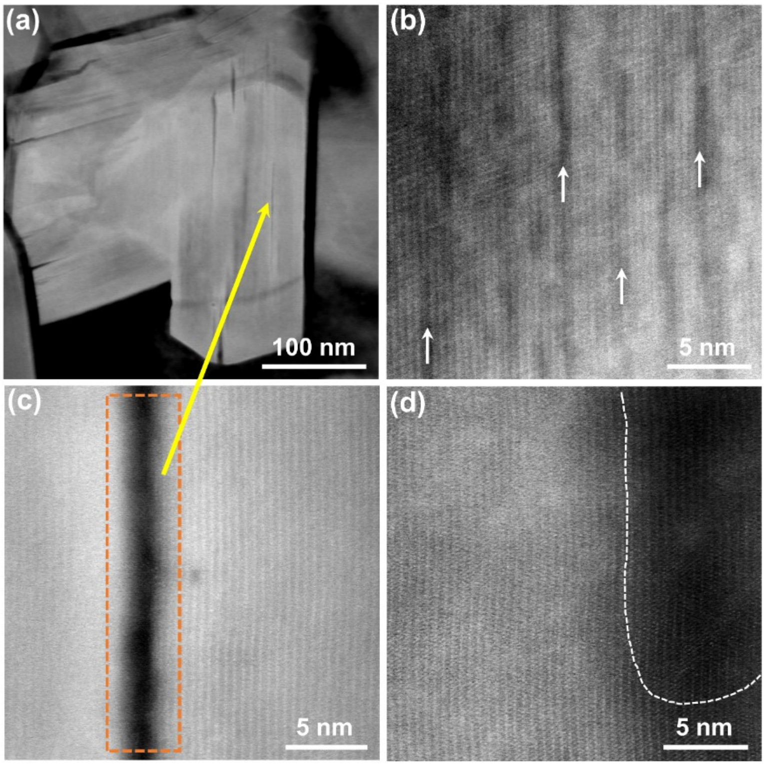

Figure S12. **(a)** Low-magnification STEM-HAADF image of the sample after 200 cycles in the voltage range of 2.0-4.3 V. **(b-d)** High resolution lattice images from the grain bulk showing the planar defects and the nano-void. (**(b-c)** intragranular cracks, **(d)** nano-void).

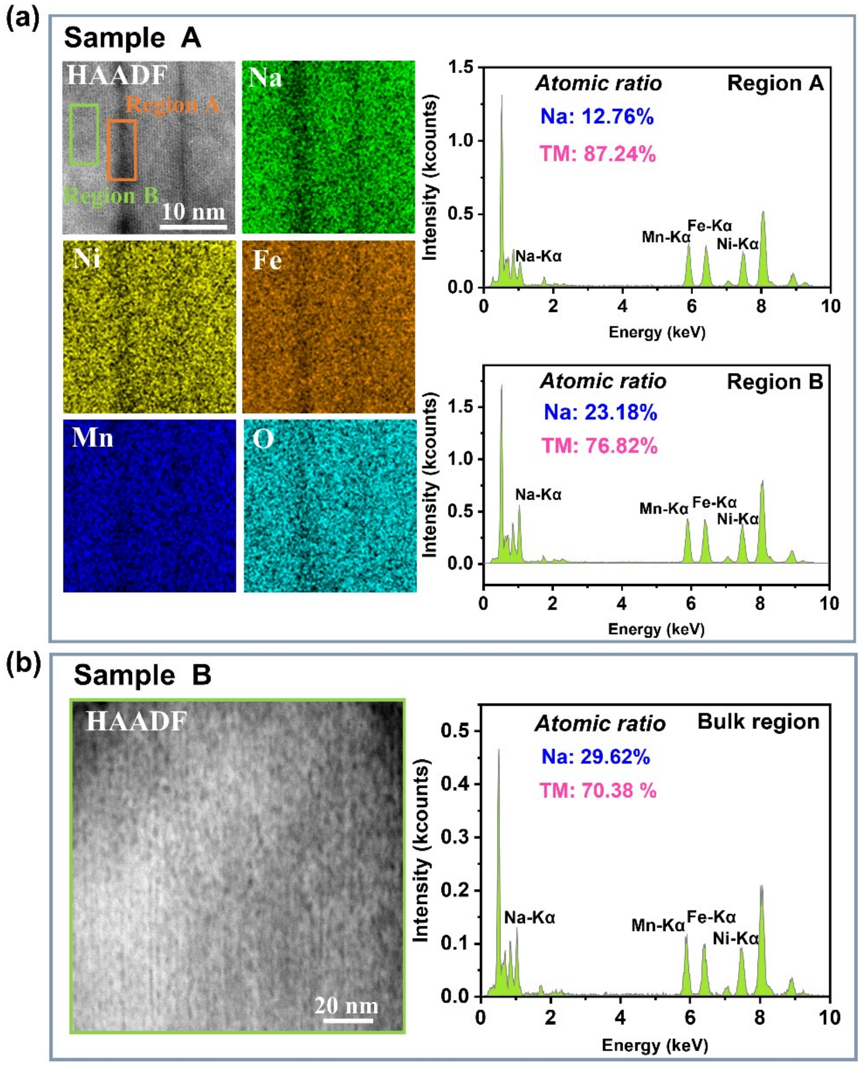

Figure S13. STEM-HAADF images, EDS elemental mappings of Na, Ni, Fe, Mn and corresponding spectra from the grain interior of sample A **(a)** and sample B **(b)**, after 200 cycles in the voltage range of 2.0-4.3 V.

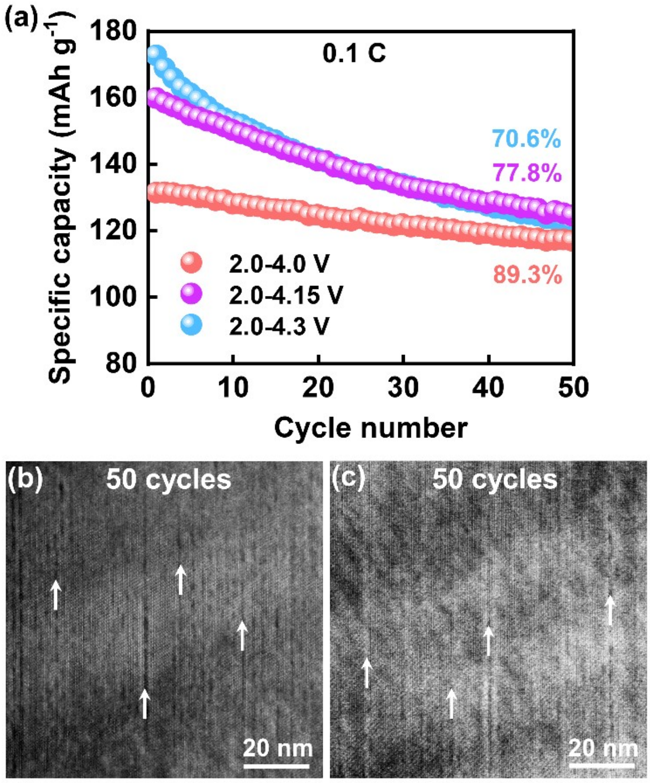

Figure S14. **(a)** The capacity retentions after 50 cycles in the voltage ranges of 2.0-4.0 V, 2.0-4.15 V and 2.0-4.3 V. **(b-c)** STEM-HAADF images of the NFM sample after 50 cycles in the voltage range of 2.0-4.3 V.

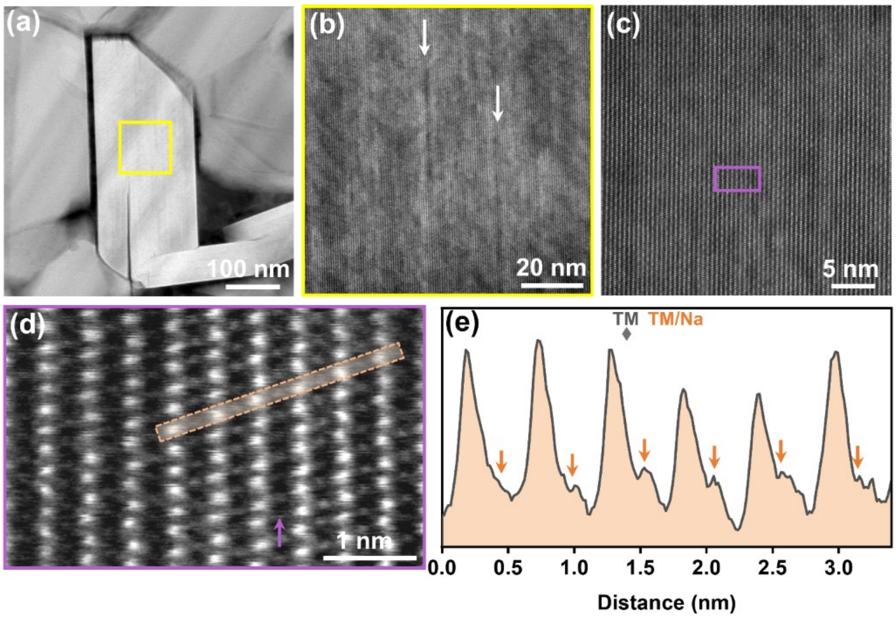

Figure S15. **(a)** Low-magnification STEM-HAADF image of the sample after 10 cycles at 2.0-4.3 V. **(b)** High resolution lattice image from the grain bulk. White arrows indicate the bulk defects. **(c)** High resolution lattice image from grain bulk. **(d-e)** Atomic-resolution STEM-HAADF image and its corresponding line profile, showing cation interlayer mixing feature.

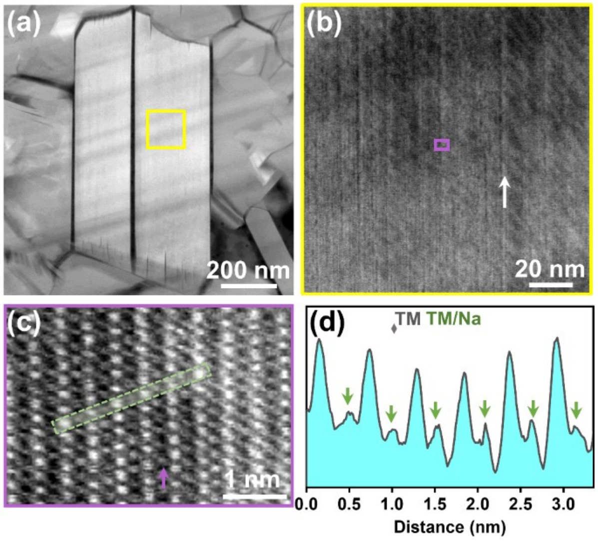

Figure S16. **(a)** Low-magnification STEM-HAADF image of the sample after 50 cycles at 2.0-4.3 V. **(b)** High resolution lattice image from grain bulk. **(c-d)** Atomic-resolution STEM-HAADF image and its corresponding line profile, showing cation interlayer mixing feature.

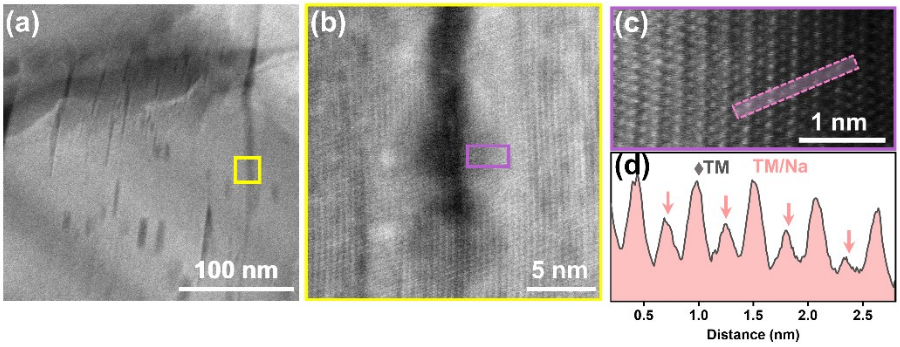

Figure S17. **(a)** Low-magnification STEM-HAADF image of the sample after 200 cycles at 2.0-4.3 V. **(b)** High resolution lattice image from the grain bulk. **(c-d)** Atomic-resolution STEM-HAADF images and their corresponding line profile, showing heavy interlayer mixing feature.

Table S1. Summary of electrochemical performance of O3-NFM in the literatures.

Cycle voltage	Initial capacity	Cycle number	Capacity retention	Reference
2.0-4.0 V	136 mAh g^{-1} (0.1 C)	100	80.5% (1 C)	1[1]
	123 mAh g^{-1} (1 C)			
2.0-4.0 V	128.0 mAh g^{-1} (0.1 C)	100	83% (1 C)	2[2]
2.0-4.0 V	130.2 mAh g^{-1} (0.1 C)	200	67% (1 C)	3[3]
	122.0 mAh g^{-1} (1 C)			
2.0-4.0 V	133.2 mAh g^{-1} (0.1 C)	200	35.4% (1C)	4[4]
2.0-4.0 V	132.0 mAh g^{-1} (0.1 C)	15	92.4% (0.1 C)	5[5]
2.0-4.0 V	125.4 mAh g^{-1} (0.1 C)	200	66.7% (1 C)	6[6]
	107.5 mAh g^{-1} (1 C)			
2.0-4.0 V	139.4 mAh g^{-1} (0.1 C)	200	53.1% (1C)	7[7]
	128.0 mAh g^{-1} (1 C)			
2.0-4.1 V	135.1 mAh g^{-1} (0.1 C)	150	46.9% (1C)	8[8]
2.0-4.3V	157.6 mAh g^{-1} (0.1 C)	15	64.4% (0.1 C)	5[5]
1.5-4.2 V	159.6 mAh g^{-1} (0.1 C)	100	58% (1 C)	9[9]
2.0-4.0 V	131.2 mAh g^{-1} (0.1 C)	200	68.8% (0.1 C)	this work
	127.4 mAh g^{-1} (0.1 C)	200	75.6% (1 C)	
2.0-4.3 V	171.5 mAh g^{-1} (0.1 C)	200	49.1% (0.1 C)	this work

Table S2. Crystallographic parameters of the NFM samples before and after 200 cycles refined by Rietveld method.

NFM	a (Å)	c (Å)	V (Å3)
Pristine	2.97159	16.00726	122.413
2.0-4.0 V	2.96626	15.99753	121.899
2.0-4.3 V	2.98153	16.15747	124.389

References:

1. H. Wang, X.-Z. Liao, Y. Yang, X. Yan, Y.-S. He and Z.-F. Ma, *J. Electrochem. Soc.*, 2016, **163**, A565-A570.
2. Y. Sun, H. Wang, D. Meng, X. Li, X. Liao, H. Che, G. Cui, F. Yu, W. Yang, L. Li and Z.-F. Ma, *ACS Appl. Energy Mater.*, 2021, **4**, 2061-2067.
3. L. Sun, Y. Xie, X. Z. Liao, H. Wang, G. Tan, Z. Chen, Y. Ren, J. Gim, W. Tang, Y. S. He, K. Amine and Z. F. Ma, *Small*, 2018, **14**, 1704523.
4. W. Wang, Y. Sun, P. Wen, Y. Zhou and D. Zhang, *J. Energy. Storage*, 2024, **79**, 110117.
5. M. Jeong, H. Lee, J. Yoon and W.-S. Yoon, *J. Power Sources*, 2019, **439**, 227064.
6. Q. Tao, H. Ding, H. Zhao, J. Huang, B. Dai and J. Li, *J. Alloys Compd.*, 2024, **976**, 172977.
7. W. Li, Q. Chen, D. Zhang, C. Fang, S. Nian, W. Wang, C. Xu and C. Chang, *Mater. Today Commun.*, 2022, **32**, 103839.
8. T. Song, L. Chen, D. Gastol, B. Dong, J. F. Marco, F. Berry, P. Slater, D. Reed and E. Kendrick, *Chem. Mater.*, 2022, **34**, 4153-4165.
9. S. Zhao, Q. Shi, R. Qi, X. Zou, J. Wang, W. Feng, Y. Liu, X. Lu, J. Zhang, X. Yang and Y. Zhao, *Electrochim. Acta*, 2023, **441**, 141859.